arXiv:1610.02019v1 [cond-mat.stat-mech] 6 Oct 2016

Enriching the dynamical phase diagram of spin chains with long-range interactions

Jad C. Halimeh[1] and Valentin Zauner-Stauber[2]

[1] *Physics Department and Arnold Sommerfeld Center for Theoretical Physics, Ludwig-Maximilians-Universität München, D-80333 München, Germany*

[2] *Vienna Center for Quantum Technology, University of Vienna, Boltzmanngasse 5, 1090 Wien, Austria*

(Dated: October 7, 2016)

Using an infinite matrix product state technique (iMPS) based on the time-dependent variational principle, we study two major types of dynamical phase transition (DPT) in the transverse-field Ising model with long-range power-law ($\propto 1/r^\alpha$ with r inter-spin distance) interactions in the thermodynamic limit – *type-I*: based on order parameters in a (quasi-)steady state, and *type-II*: based on nonanalyticities (cusps) in the Loschmidt-echo return rate. We construct the corresponding rich dynamical phase diagram, whilst considering different quench initial conditions. We find a nontrivial connection between both types of DPT based on their critical lines. Moreover, we observe a new type-II dynamical phase in a certain range of interaction exponent α, characterized by what we call *anomalous cusps*, which are distinct from the regular cusps usually associated with a type-II DPT. We illustrate the transition between these two groups of cusps through the rate-function branches of the iMPS transfer matrix, which is a major strength of this method for studying the type-II DPT. Our results provide the characterization of experimentally-accessible signatures of the dynamical phases studied in this work.

I. INTRODUCTION

Phase transitions are among the most fascinating phenomena in physics whereby a small change in a control parameter of the system can drive the system between extremely different phases that are not adiabatically connected to one another, thus giving rise to nonanalyticity in the free energy even when the system itself is described by a completely analytic Hamiltonian with no singularities. Quantum and classical equilibrium phase transitions are textbook subjects that have been very well studied and established in various systems. Recently, and particularly in the context of closed quantum systems, quench dynamics[1] and post-quench system behavior has received a lot of attention. Of special interest is the concept of dynamical phase transitions (DPTs), where, for one type of such DPTs, critical behavior is inspected in a post-quench (quasi-)steady state, such as a prethermal state at intermediate times, or steady state that looks locally thermal in case of thermalization in a nonintegrable system, in some cumulant (such as e.g. the order parameter or variance thereof) as a function of some control parameter in the quenching Hamiltonian. This type-I DPT is particularly interesting in the sense that it is shown to exist in models where the corresponding finite-temperature equilibrium phase transition is absent.[2] Reaching a quasi-steady state is crucial in this DPT in order to extract a steady-state value of the cumulant under consideration. On the other hand, there is the type-II DPT, which, in addition to the seminal work[3] defining it, has been extensively studied analytically[4–8] and numerically[9,10] in several models, and just recently even observed experimentally[11] in the dynamics of a fermionic many-body state after a quantum quench. Similar to the type-I DPT, the type-II DPT also involves a quench between an initial and a final Hamiltonian, however, unlike the type-I DPT, (pre)thermalization is not a requirement, not least because the type-II DPT actually manifests itself as a nonanalyticity in the Loschmidt-echo return rate[3] as a function of evolution time. In general, the type-II DPT occurs when an initial state at $T = 0$ undergoes a quench between two Hamiltonians such that the control parameter that effects this quench crosses the equilibrium critical point,[3–5] and has been observed in the nearest-neighbor transverse field Ising model (TFIM) with quenches across the quantum equilibrium critical point from both phases.[3,5] However, there have been exceptions to this general rule, where a type-II DPT does occur for quenches within the same phase and is absent in quenches across the quantum equilibrium critical point,[12,13] and it has been shown that the type-II DPT is absent in the nearest-neighbor transverse field Ising model(NN-TFIM) at $T > 0$.[14]

We have shown in a related work with colleagues,[2] that the type-I DPT in the long-range TFIM might exist in situations even when the system under consideration does not exhibit a finite-temperature phase transition.[15] For further details, we refer the reader to Ref. 2. In this paper, we shall focus on the behavior of the type-II DPT, how we detect it in the framework of infinite matrix product states (iMPS)[16,17] in the thermodynamic limit, and characterizing its different phases. We find that it is extremely beneficial to work with iMPS here as opposed to finite-size time-dependent density matrix renormalization group (t-DMRG) methods.[18–20] As we shall see later, and as shown in the seminal works[3,5] in the nearest-neighbor TFIM, the type-II DPT manifests itself as nonanalyticities in the form of cusps in some analogue of the free energy. Due to finite size effects, these cusps will be smoothened out in finite systems, thus indicating no nonanalyticity (and thus no criticality) in the free energy analogue. One can in principle use finite-size scaling in order to surmise a cusp in the thermodynamic limit, but such a method might be error-prone, cumber-

some, and requires unrealistic numerical resources. In iMPS, on the other hand, we *a priori* deal with an infinite system, and one can directly see sharp cusps in the free energy analogue. Moreover, as explained in detail in Sec. A, the type-II DPT can be very straightforwardly detected from level crossings in the eigenvalues of the MPS transfer matrix.

Naturally, several questions arise in the context of these DPTs in the long-range TFIM, such as whether or not type-I and type-II DPTs are related, the particular phase diagram that can be constructed from studying the quantum quenches that give rise to these DPTs, proper characterization of the dynamical phases within, and what signatures would be experimentally feasible to detect. In this paper, it is exactly these questions that we study, and a summary of our results can be found in Fig. 1. The paper is organized as follows: In Sec. II we briefly review the theory of the type-II DPT and discuss its detection in the framework of iMPS. In Sec. III we present the main results of this study and discuss them. We conclude in Sec. V.

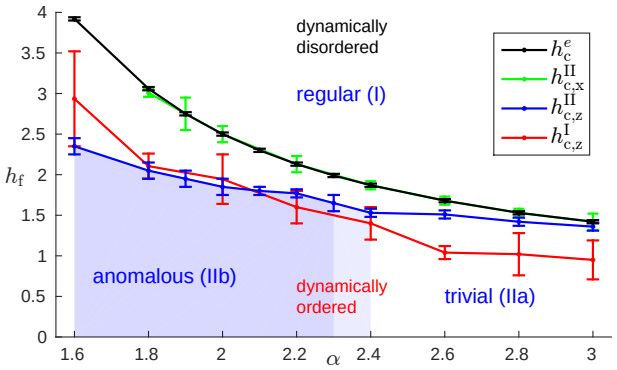

Figure 1. Enriched dynamical phase diagram of the long-range TFIM. h_c^e is the equilibrium critical line, $h_{c,z}^{I}$ is the type-I dynamical critical line, $h_{c,z}^{II}$ is the type-II dynamical critical line for quenches from $h_i = 0$ which signifies the onset of *regular cusps* for quenches above it, $h_{c,x}^{II}$ is the type-II dynamical critical line for quenches from $h_i \to \infty$ (there are no anomalous cusps for these quenches). Note how the critical lines $h_{c,x}^{II}$ and h_c^e overlap very well within the precision of our numerical simulations. For quenches from $h_i = 0$ to below $h_{c,z}^{II}$, the system ends up in a trivial (cusp-free) phase for $\alpha \gtrsim 2.3$ and an anomalous phase for $\alpha \lesssim 2.3$.

II. TYPE-II DPT

We consider the long-range transverse-field Ising model with power-law interactions

$$\mathcal{H} = -J \sum_{j>i=1}^{L} \frac{\sigma_i^z \sigma_j^z}{|i-j|^\alpha} - h \sum_i \sigma_i^x, \tag{1}$$

where $\sigma_i^{x,z}$ are Pauli matrices acting on site i, $J > 0$ is the spin-spin coupling constant, h is the magnetic field, L is the number of sites and we consider the thermodynamic limit $L \to \infty$. For quenches whose time evolution is propagated by $\mathcal{H}$, the motivation[3] for studying nonanalyticities in the Loschmidt echo

$$G(t) = \langle \psi(0)|\psi(t)\rangle = \langle \psi(0)|e^{-\mathrm{i}\mathcal{H}t}|\psi(0)\rangle \tag{2}$$

is to exploit the similarity between (2) and the partition function of the system in thermal equilibrium at inverse temperature β

$$\mathcal{Z}(\beta) = \mathrm{Tr}\, \mathrm{e}^{-\beta\mathcal{H}}, \tag{3}$$

and interpret (2) as a boundary partition function with boundary conditions $|\psi(0)\rangle$ and complex inverse temperature z

$$\mathcal{Z}_b(z) = \langle \psi(0)|e^{-z\mathcal{H}}|\psi(0)\rangle \tag{4}$$

along the imaginary axis $z = \mathrm{i}t$. Thus, the logarithm of the return probability $P(t) = |G(t)|^2$, i.e. the *return rate function*

$$r(t) = -\lim_{L\to\infty} \frac{1}{L} \log |G(t)|^2, \tag{5}$$

can be construed as an analogue of the free energy per site, in which nonanalyticities indicate the presence of a type-II DPT. Here one basically makes a connection between finite-temperature partition functions and time evolution, asking whether the latter can exhibit phase transitions as well. The type-II DPT has been studied in various systems, and in the case of the transverse-field Ising model (TFIM), it has been shown for the integrable cases of nearest-neighbor[3,5] ($\alpha \to \infty$) and infinite-range interactions ($\alpha = 0$).[8] In this paper, we study the type-II DPT in the one-dimensional long-range interacting ($1 < \alpha < \infty$), nonintegrable TFIM in the thermodynamic limit.

To study the type-II DPT, we calculate the return rate function per site[3] (5), after performing a quantum quench, where we prepare the system in the groundstate $|\psi(0)\rangle$ of $\mathcal{H}(h_i)$ (that is $h = h_i$ in (1)), and then abruptly change the magnetic field from h_i to $h_f \neq h_i$ at time $t = 0$. As the system evolves in time as propagated by $\mathcal{H}(h_f)$, the return rate function per site (5) can then be calculated from the overlap (2) of the initial state with its time-evolved self. The return rate function can be calculated efficiently directly in the thermodynamic limit with iMPS techniques (minus) the logarithm of the dominant eigenvalue of an MPS transfer matrix at time t. Cusps in the return rate occur when there is a level crossing of the dominant eigenvalues of this transfer matrix. For details see Sec. A 3.

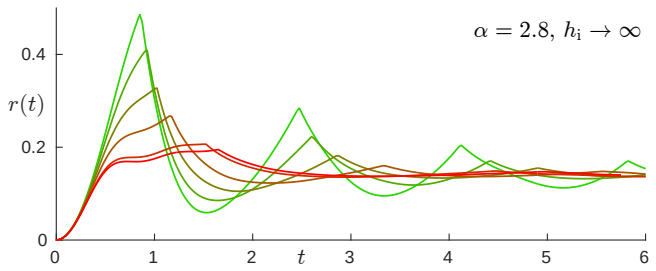

Figure 2. Return-rate function $r(t)$ for $\alpha = 2.8$, quenches from $h_i \to \infty$ to $h_f \in [0.75, 1.40]$ (from green to red).

III. RESULTS AND DISCUSSION

We shall now discuss the results of our iMPS time-evolution simulations for two types of quenches in the long-range TFIM (1) and first extract signatures of criticality for type-II DPT: (i) A quench from $h_\mathrm{i} \to \infty$, corresponding to an initial state, which is the completely polarized state in positive x-direction (X-quench), and (ii) a quench from $h_\mathrm{i} = 0$, where the groundstate is two-fold degenerate. We choose the completely polarized state in the positive z-direction as initial state (Z-quench).

For the X-quenches we find a critical phase, with the occurrence of conventional cusps in the return rate (5), as first observed in the nearest-neighbor transverse field Ising model (NN-TFIM).[3] Henceforth, these cusps will be called *regular* cusps. We also find a trivial phase with no cusps in the return rate. These two phases exist for all studied α. For Z-quenches we again find a regular and a trivial phase, but additionally encounter an anomalous phase, replacing the trivial phase for $\alpha \lesssim 2.3$ only. The *anomalous* cusps appearing in this phase are qualitatively different from the regular ones. Lastly, signatures of criticality for the type-I DPT, studied and characterized in Ref. 2, are also included for comparison. See Fig. 1 for the enriched phase diagram.

First, let us consider the case of X-quenches to some final value h_f of the transverse field, where we encounter the same situation as for the NN-TFIM.[3] For quenches within the disordered *equilibrium* phase $h_\mathrm{f} > h_\mathrm{c}^\mathrm{e}(\alpha)$, with $h_\mathrm{c}^\mathrm{e}(\alpha)$ the quantum equilibrium critical line,[21–23] we observe a trivial phase with no cusps at all in the return rate. However, quenching across $h_\mathrm{c}^\mathrm{e}(\alpha)$ into the ordered equilibrium phase, we encounter a regular critical phase and (regular) cusps appear. Fig. 2 shows an example for $\alpha = 2.8$ and various h_f across the equilibrium critical point. It is apparent that the deeper the quench into the ordered phase, the more pronounced the cusps are, and the smaller the time intervals between the cusps become. As the quench approaches the critical point from below, these cusps appear less sharp and the intervals between them get longer. All cusps completely disappear simultaneously when crossing $h_\mathrm{c}^\mathrm{e}(\alpha)$ from below, i.e. when quenching within the disordered phase. The similarity to the NN-TFIM case is indicated in Fig. 1 by the overlap of the type-II dynamical critical line $h_\mathrm{c,x}^\mathrm{II}$ for X-quenches with the quantum equilibrium critical line h_c^e within the precision of our numerical simulations.

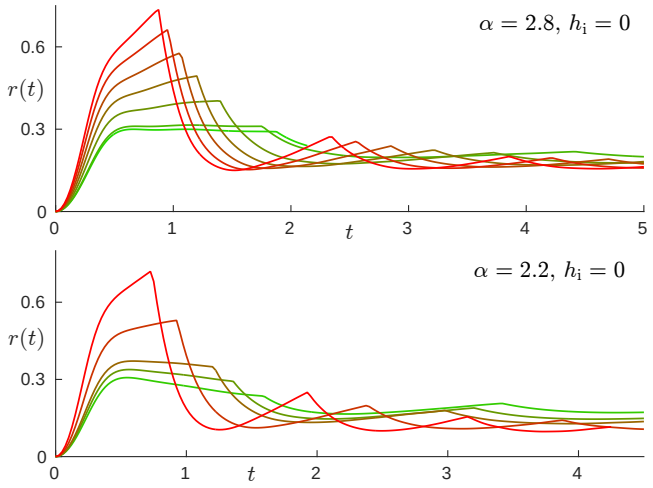

Figure 3. Return-rate function $r(t)$ for quenches from $h_\mathrm{i} = 0$ to $h_\mathrm{f} \in [1.50, 2.30]$ (from green to red) for $\alpha = 2.8$ (top) and $h_\mathrm{f} \in [1.80, 2.80]$ (from green to red) for $\alpha = 2.2$ (bottom). This behavior is qualitatively the same for all α.

On the other hand, for Z-quenches, we see three distinct type-II dynamical phases: (I) a *regular phase* with only regular cusps in the return rate (as for X-quenches above), that occurs when quenching across a type-II dynamically critical field value $h_\mathrm{c,z}^\mathrm{II}(\alpha)$, which is however lower than h_c^e (c.f. Fig. 1). For quenches below $h_\mathrm{c,z}^\mathrm{II}(\alpha)$ we encounter (IIa) a *trivial phase* for $\alpha \gtrsim 2.3$, that exhibits no cusps at all in the return rate, and interestingly, (IIb) an *anomalous* phase for $\alpha \lesssim 2.3$, that exhibits in the return rate anomalous cusps that are qualitatively different from the regular cusps in phase (I). The phase diagram in Fig. 1 therefore gets enriched in the regime $h_\mathrm{f} < h_\mathrm{c,z}^\mathrm{II}$. The additional appearance of phase (IIb) featuring anomalous cusps and a critical field $h_\mathrm{c,z}^\mathrm{II}(\alpha)$ different from $h_\mathrm{c}^\mathrm{e}(\alpha)$ for this quench are the two major differences to such a quench in the NN-TFIM.

Let us focus on the regular phase (I) first. In Fig. 3 we show results for quenches to various $h_\mathrm{f} > h_\mathrm{c,z}^\mathrm{II}$ and various α, where cusps in the rate function appear in roughly equispaced time intervals. With lowering h_f and approaching $h_\mathrm{c,z}^\mathrm{II}$, these time intervals *increase* and the cusps get less and less sharp until they all vanish simultaneously when crossing $h_\mathrm{c,z}^\mathrm{II}$. The time intervals as a function of h_f seem to be largely independent of α (see Fig. 4). These time intervals are also reflected in the oscillation period of the order parameter $m(t) = \langle \sigma^z(t) \rangle$. The times at which regular cusps appear match the zero crossings of $m(t)$ up to a temporal shift, as shown in Fig. 5. This fact has already been observed in the NN-TFIM[3,10] and next-nearest-neighbor TFIM.[10] It is worthy to note here that the periodicity of the return rate is doubled[3,10] if one considers the return rate with respect to the degenerate

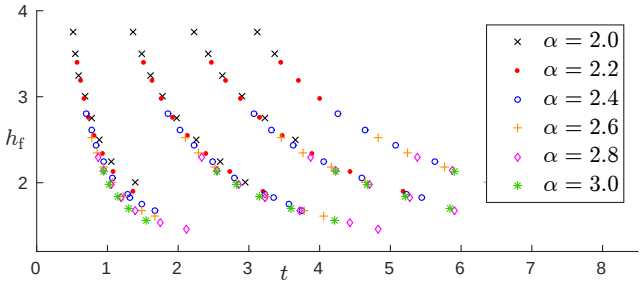

Figure 4. Times of regular cusps (c.f. Fig. 3 bottom), appearing in quenches from $h_\mathrm{i} = 0$, for various $\alpha \in [2, 3]$ and $h_\mathrm{f} > h_\mathrm{c,z}^\mathrm{II}$. It is clearly visible, that the respective times of the cusps *decrease* with increasing h_f. Moreover, the dependence of the times for each cusp seems independent of α, within an uncertainty of $\approx 5\%$.

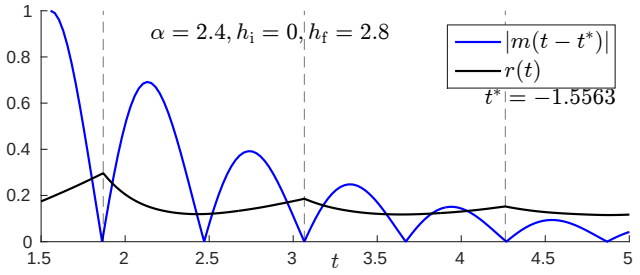

Figure 5. Return rate function $r(t)$ plotted together with (absolute value of) order parameter $|m(t)|$. The zeros of the shifted order parameter coincide with the cusps in the return rate.

subspace of the initial state rather than the initial state itself as we do. Thus, the only difference of this phase to conventional type-II criticality in the NN-TFIM is the critical field $h_\mathrm{c,z}^\mathrm{II}$.

The regular critical phase goes over into an anomalous critical phase (IIb) for quenches below $h_\mathrm{c,z}^\mathrm{II}$ and $\alpha \lesssim 2.3$. There, after a coexistence with the regular cusps around $h_\mathrm{c,z}^\mathrm{II}$, a qualitatively different type of cusps in the rate function appears (see Fig. 6). Upon further lowering h_f, the time intervals between these cusps *decreases*, contrary to the regular cusps in phase (I), and they vanish one by one as $h_\mathrm{f} \to 0$, starting at early times, as can be seen in Fig. 7. As our evolution times for accurate simulations are limited, we can only conjecture that this type of cusps exists for any small $h_\mathrm{f} > 0$, albeit only appearing at very large times. It is worth mentioning that some of these anomalous cusps show a "double-cusp" structure, where the location of these double cusps also seems to drift with α (for examples see Sec. B 1). It also appears that these double cusps vanish sooner with lowering h_f than a preceding cusp. The nature and origin of these double cusps remains elusive. Such double cusps have previously been observed also for the transverse axial next-nearest-neighbor (ANNNI) and tilted field Ising model.[10]

Reiterating in comparison, upon lowering h_f the time intervals between regular cusps increases, whereas they decrease between anomalous cusps. Also, the regular cusps all vanish simultaneously when crossing $h_\mathrm{c,z}^\mathrm{II}$ (after a short coexistence region), whereas the anomalous cusps vanish one by one as $h_\mathrm{f} \to 0$. Finally, the time intervals between anomalous cusps as a function of h_f shows a clear α-dependence, whereas for regular cusps the intervals seem to be largely independent of α (see Fig. 4 and Fig. 7).

For quenches below $h_\mathrm{c,z}^\mathrm{II}$ and $\alpha \gtrsim 2.3$, the regular phase (I) goes over into a trivial phase (IIa) with no cusps in the return rate.

We emphasize here that the two types of observed cusps are qualitatively different, as can be seen in how they arise from two qualitatively different groups of rate-function branches (A7) calculated from the MPS transfer matrix (A6), where it is always the lowest branch that corresponds to the actual return rate function. For $h_\mathrm{f} > h_\mathrm{c,z}^\mathrm{II}$ the lowest rate-function branches are those developing regular cusps by crossing each other over time. Moving h_f closer and below $h_\mathrm{c,z}^\mathrm{II}$, this group of branches moves further up, revealing another (now lowest) group of rate-function branches developing anomalous cusps for $\alpha \lesssim 2.3$, or a group of branches without any crossings – and thus no cusps – for $\alpha \gtrsim 2.3$. These different groups of rate-function branches can in principle be distinguished by their functional form in time and the dependence of the time intervals between the crossings on h_f. For further details on the crossover between the regular phase (I) and the anomalous phase (IIb), see Sec. B 2.

It would be interesting to know if the physical origin of these two different types of cusps is due to two different groups of Fisher zero lines of (4) in the complex plane,[3] crossing the imaginary axis in different ways.

To summarize our findings for Z-quenches, in addition to the regular type-II critical phase (I) for $h_\mathrm{f} > h_\mathrm{c,z}^\mathrm{II}$ and all α, and the trivial phase (IIa) for $h_\mathrm{f} < h_\mathrm{c,z}^\mathrm{II}$ and $\alpha \gtrsim 2.3$, we also find an anomalous phase (IIb) for $h_\mathrm{f} < h_\mathrm{c,z}^\mathrm{II}$ and $\alpha \lesssim 2.3$. This is surprising, as in the anomalous phase we encounter cusps without quenching across $h_\mathrm{c,z}^\mathrm{II}$, i.e. when quenching within the same phase. The cusps in the regular and anomalous phase differ qualitatively in their form, the time intervals between them, and how they vanish upon lowering h_f.

Finally, after characterizing the type-II DPT for X-quenches and Z-quenches and observing a new type-II phase due to anomalous cusps, we discuss the relationship of the type-I and type-II DPTs according to their critical lines in the rich phase diagram of Fig. 1. The critical line of the type-I DPT is much harder to obtain, as this kind of DPT relies on reaching a kind of a steady state at time $t \approx t^*$, from which the order parameter $\tilde{m} = m(t^*)$ is extracted, and then one tries to establish the existence or absence of a nonanalyticity of this order parameter as a function of h_f, as in our case. This type-I DPT has been extensively studied in the nonintegrable long-range TFIM,[2] and it was estab-

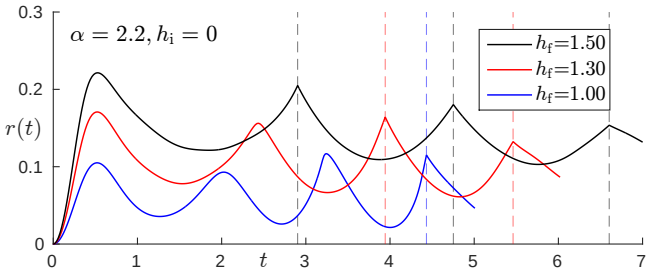

Figure 6. Examples of anomalous cusps (marked by vertical dashed lines) for $h_f < h_{c,z}^{II}$. It is clearly visible, that with increasing h_f more and more such cusps develop at smaller and smaller times, their respective locations however move to higher times (c.f. also Fig. 7). See Fig. 9 for a plot showing how these cusps arise from level crossings in the MPS transfer-matrix.

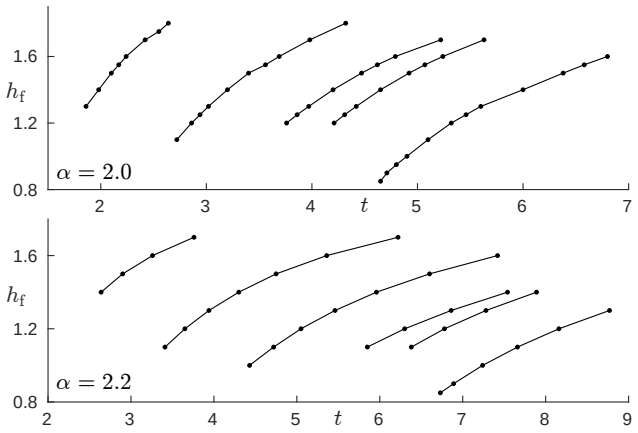

Figure 7. Times of anomalous cusps only, for $\alpha = 2$ (top) and $\alpha = 2.2$ (bottom) as a function of $h_f < h_{c,z}^{II}$. For $h_f > h_{c,z}^{II}$, the anomalous cusps vanish, as the regular cusps take over. The shown black lines would continue further to higher times (top right), but were outside our reachable simulation times.

lished that pre-thermalization conspires to give rise to the type-I DPT even for $\alpha > 2$ where the long-range TFIM exhibits no thermal phase transition in one spatial dimension.[15] Comparing the type-I and type-II critical lines, an unequivocal conclusion is unrealistic, given the evolution times of accurate simulations reached, or by those also done using finite-size t-DMRG.[2] However, from the data, it looks that the two types of DPT are nontrivially connected and at least show the same tendency in their α-dependence.

IV. CONCLUSIONS

We have carried out time-evolution simulations of pure quantum states after quantum quenches in the one-dimensional long-range TFIM in the thermodynamic limit using an iMPS technique based on the time-dependent variational principle. We considered different initial conditions for the quantum quenches and studied two corresponding types of dynamical phase transition: the type-I DPT characterized by a nonanalyticity in the magnetization of a dynamical quasi-steady state as a function of the transverse-field strength, and the type-II DPT manifested as nonanalyticities in the form of cusps in the Loschmidt-echo return rate. For the type-II DPT, quenches from the fully x-polarized state (X-quenches) lead to two dynamical phases separated by the quantum equilibrium critical line, where the return rate exhibits cusps only for quenches into the ordered equilibrium phase. These cusps resemble in their nature those already found and studied in the nearest-neighbor TFIM. On the other hand, for Z-quenches, where the initial state is fully z-polarized, when quenching into the disordered dynamical phase we observe conventional (regular) cusps for all α, where we have calculated the corresponding dynamical critical line, which differs from the equilibrium critical line. For Z-quenches below this dynamical critical line, we find two phases: the trivial cusp-free phase for $\alpha > 2.3$ similar to that found in the case of the nearest-neighbor TFIM or in the case of X-quenches in the long-range TFIM, and, quite remarkably, a third distinct anomalous phase for $\alpha \lesssim 2.3$ where the return rate shows anomalous cusps that may be the result of a different group of Fisher zero lines of the partition function in the complex plane. Finally, we also show a nontrivial connection between the type-I and type-II DPTs, albeit with the precision of our numerical simulations, this connection cannot be reasonably described as definitive.

In the final stages of writing this manuscript, we became aware of a study[24] that discusses some of our results in part while dealing with finite-size systems.

ACKNOWLEDGMENTS

Both authors contributed equally to this work. We thank Damian Draxler, Jutho Haegeman, Michael Kastner, Andreas Läuchli, Ian P. McCulloch, Francesco Piazza, and Frank Verstraete for inspiring and helpful discussions. V. Z.-S. gratefully acknowledges support from the Austrian Science Fund (FWF): F4104 SFB ViCoM and F4014 SFB FoQuS.

Appendix A: Infinite matrix product state technique

In this section we give a short description of the algorithm used to simulate the real-time evolution of a spin chain under a Hamiltonian with long-range interactions in the thermodynamic limit. In our case, this Hamiltonian is the long-range TFIM, but our algorithm applies to other general models.

1. Long-range interactions

We assume the Hamiltonian to contain a sum of two-body interactions of the form $h^{(2)}_{ij} = O_i O_j f(|j-i|)$, where operators O_i act on a single site i and commute when acting on different sites $[O_i, O_j] = 0$, $i \neq j$. Specifically, we consider the long-range transverse-field Ising model (1), where the distance function decays as a power law $f(n) = n^{-\alpha}$ and we assume $f(n)$ to be well approximated by a sum of K exponentials, i.e. $f(n) = \sum_{k=1}^{K} c_k \lambda_k^{n-1}$, with $\lambda_k < 1$ and $n > 0$. With this approximation the overall Hamiltonian is then given by

$$\mathcal{H} = -J \sum_k \sum_{j>i} c_k \lambda_k^{j-i-1} \sigma_i^z \sigma_j^z - h \sum_i \sigma_i^x. \tag{A1}$$

For an infinite system we fit $f(n)$ with a suitable number of exponentials over a distance N large enough, such that $f(N) < \varepsilon_f$, where ε_f is of the order $\mathcal{O}(10^{-6})$ - $\mathcal{O}(10^{-8})$ and the largest residuals are of the order $\mathcal{O}(10^{-5})$. This usually amounts to a K in the range of $5 - 25$.

2. MPS real-time evolution

To simulate the real-time evolution of a pure quantum state $|\psi\rangle$ within the variational space of Matrix Product States (MPS)[16,17,25] with respect to (A1), we adapt the algorithm of Ref. 26 to the thermodynamic limit. The method of Ref. 26 integrates the time-dependent Schrödinger equation $\partial_t |\psi\rangle = -\mathrm{i}\,\mathcal{H}\,|\psi\rangle$ by applying the time-dependent variational principle (TDVP) onto the subspace of MPS,[27] but uses a Lie-Trotter splitting scheme of the projector onto the tangent space of the variational manifold to directly integrate the effective differential equations for the MPS tensors. Due to this splitting scheme it is necessary to evolve the state in small time steps τ only. For details on notation and the algorithm we refer the reader to Refs. 26 and 27.

In the following we describe the evolution of a translation-invariant MPS in the thermodynamic limit (iMPS) by a small time step τ. We assume the state at time t to be given in terms of a translation-invariant iMPS in the mixed canonical form,[25] i.e. the state is approximated by an MPS given by (site-independent) MPS tensors A^s_L and A^s_R in the left and right gauge, and a bond matrix C whose singular values are the Schmidt-values of a bipartition of the state

$$|\psi\rangle = \sum_{\mathbf{s}} (\ldots A_L^{s_{n-2}} A_L^{s_{n-1}} C A_R^{s_n} A_R^{s_{n+1}} \ldots) |\mathbf{s}\rangle\,, \tag{A2}$$

where n is an arbitrary site on the chain. This also defines a center-tensor $A^s_C = A^s_L C = C A^s_R$ and the gauge conditions read

$$\sum_s {A^s_L}^\dagger A^s_L = \mathbb{1} \qquad \sum_s A^s_L C C^\dagger {A^s_L}^\dagger = C C^\dagger \tag{A3}$$

$$\sum_s A^s_R {A^s_R}^\dagger = \mathbb{1} \qquad \sum_s {A^s_R}^\dagger C^\dagger C\, A^s_R = C^\dagger C. \tag{A4}$$

We represent the Hamiltonian (A1) in terms of a Matrix Product Operator (MPO)[28–31] W with bond dimension $d_w = K + 2$. The projection of $\mathcal{H}\,|\psi\rangle$ onto the MPS tangent plane defines effective Hamiltonians H for A^s_C and K for C[26]. In order to calculate these it is necessary to determine the left and right fixed points of the MPO transfer matrices (c.f. Ref. 32 and Fig. 8)

$$\mathcal{T}^{ab}_{L/R} = \sum_{ss'} W^{ab}_{s's} \bar{A}^{s'}_{L/R} \otimes A^s_{L/R}, \tag{A5}$$

where a bar denotes complex conjugation and indices $a, b \in [1, \ldots, d_w]$.

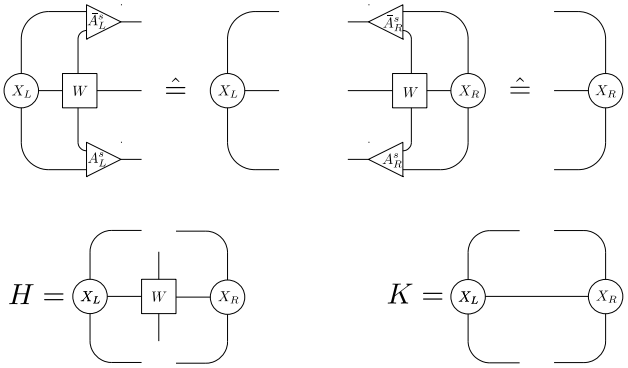

Figure 8. Fixed point relations for the left and right MPO transfer matrices (A5) and definition of the effective Hamiltonians H for A^s_C and K for C. The symbol $\hat{=}$ refers to equality up to terms contributing to the energy expectation value per site[32].

The algorithm in Ref. 26 for a *finite* chain proceeds by performing the following steps sequentially for each site n of the lattice (e.g. in a left-to-right sweep)

1. Calculate $H(n)$ as a function of $\tilde{A}^s_L(m < n)$ and $A^s_R(m > n)$.
2. Evolve $\tilde{\mathbf{A}}_C(n) = \exp(-\mathrm{i}\tau\, H(n))\, \mathbf{A}_C(n)$ forwards in time.
3. Split $\tilde{A}^s_C(n) = \tilde{A}^s_L(n)\, \tilde{C}(n)$.
4. Calculate $K(n)$ as a function of $\tilde{A}^s_L(m \leq n)$ and $A^s_R(m > n)$.

5. Evolve $\mathbf{C}(n) = \exp(+\mathrm{i}\tau\, K(n))\, \tilde{\mathbf{C}}(n)$ *backwards* in time and form $A_C^s(n+1) = C(n)\, A_R^s(n+1)$.

Here $\tilde{A}_L^s(n)$ refers to tensors updated in previous steps and bold symbols refer to vectorizations of the tensors. Note that both H and K are calculated from *evolved* $\tilde{A}_L^s$ and yet unevolved A_R^s. In the thermodynamic limit, A_L^s and A_R^s correspond to the same state and we want to evolve both of them at the same time. The following adapted algorithm achieves this

1. Calculate H and K from current A_L^s and A_R^s and form $A_C^s = A_L^s C = C A_R^s$.

2. Evolve $\tilde{\mathbf{A}}_C = \exp(-\mathrm{i}\tau\, H)\, \mathbf{A}_C$ forwards in time.

3. Evolve $\tilde{\mathbf{C}} = \exp(-\mathrm{i}\tau\, K)\, \mathbf{C}$ *forwards* in time.

4. Determine the optimal updated $\tilde{A}_L^s$ and $\tilde{A}_R^s$ by minimizing $\varepsilon_R = \|\sum_s \tilde{A}_C^s - \tilde{A}_L^s \tilde{C}\|_2$ and $\varepsilon_R = \|\sum_s \tilde{A}_C^s - \tilde{C}\tilde{A}_R^s\|_2$ under the constraints $\sum_s \tilde{A}_L^{s\dagger}\tilde{A}_L^s = \sum_s \tilde{A}_R^s \tilde{A}_R^{s\dagger} = \mathbb{1}$.

This scheme corresponds to a first-order splitting scheme[33] with an error scaling of $\mathcal{O}(\tau^2)$.[26] In practice we use a time step of $\tau = 0.002$. The quantities ε_L and ε_R can be used as a measure of the quality of a time step and of the constraint $A_L^s C = C A_R^s$. We regauge the state if ε_L and ε_R rise above a certain threshold.

We increase the bond dimension of the MPS whenever the smallest of the Schmidt-values (which are the singular values of C) rises above a certain threshold ε_S. For this we use a variant of a single application of the two-site integrator presented in Ref. 26, adapted to the thermodynamic limit.[34] In practice we use $\varepsilon_S = 10^{-9}$ and a maximum bond dimension of $D_{\max} \approx 350$, which – depending on $\mathcal{H}$ – limits the maximum reachable simulation time $t_{\max}$ severely due to the (at worst) linear increase of entanglement entropy[35,36].

3. Loschmidt echo and the return rate

The rate function of the return probability per site (5) corresponds to (minus) the logarithm of the dominant eigenvalue of the mixed MPS transfer matrix[10]

$$\mathcal{T}(t) = \sum_s \bar{A}^s(0) \otimes A^s(t) \tag{A6}$$

between MPS tensors[37] at time zero and t, whose spectral radius is $\rho(\mathcal{T}(t)) \leq 1$. If $\epsilon_i(t)$ are the eigenvalues of (A6) in descending order by magnitude (i.e. $\epsilon_1(t)$ being the largest), then we define the rate-function branches

$$r_i(t) = -2 \log |\epsilon_i(t)|, \tag{A7}$$

and the rate function (5) is simply $r(t) = r_1(t)$, with all other $r_{i>1} > r_1(t)$.

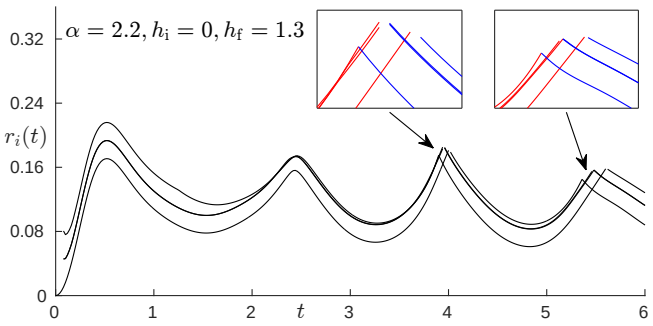

Figure 9. Example of how cusps in the return rate $r(t)$ can be detected through level crossings of the rate-function branches $r_i(t)$ (A7). Shown are the first four $r_i(t)$ for a quench from $h_\mathrm{i} = 0$ to $h_\mathrm{f} = 1.3$ and $\alpha = 2.2$, where the *lowest* branch represents the rate function (5). At $t \approx 2.4$ there are no level crossings, $r(t)$ is thus smooth. At times $t \approx 4$ and $t \approx 5.5$ there are level crossings in the rate-function branches, which cause cusps in $r(t)$. The example shows anomalous cusps, however also regular (or in fact any other type of) cusps show up due to this mechanism. The insets show a magnification of these cusps, where branches that are going up are colored red and branches coming down are colored blue for better visualization.

Nonanalyticities of (5) in t in the form of cusps arise due to level crossings in the eigenspectrum of (A6), which is a feature characteristic of first-order phase transitions. The occurrence of such nonanalyticities can thus nicely be anticipated by calculating and following the first few rate-function branches. Cusps arise at branch crossings, where a higher branch becomes the lowest one at some time t_c (see Fig. 9).

The mixed MPS transfer matrix (A6) represents a renormalized version of the true Quantum Transfer Matrix of a real-time path-integral formulation of (2).[38]

4. Alternative calculation of the rate function

Trivially, (2) can also be written as

$$\begin{aligned}\langle\psi(0)|\psi(t)\rangle &= \langle\psi(0)|\exp(-i\mathcal{H}t)|\psi(0)\rangle \\ &= \left(\langle\psi(0)|\exp(-i\mathcal{H}t/2)\right)\left(\exp(-i\mathcal{H}t/2)\,|\psi(0)\rangle\right) \\ &= \langle\psi(-t/2)|\psi(t/2)\rangle\,, \end{aligned} \tag{A8}$$

where in the present case the backward-evolved state $|\psi(-t/2)\rangle$ can be obtained from the forward-evolved state as $|\psi(-t/2)\rangle = \overline{|\psi(t/2)\rangle}$, i.e. by complex conjugation. We exploit this fact to evaluate the rate function at time t with the MPS at time $t/2$, i.e. we use the leading eigenvalues of

$$\tilde{\mathcal{T}}(t) = \sum_s A^s(t/2) \otimes A^s(t/2). \tag{A9}$$

Thus, $r(t)$ can be calculated both from (A6) at time t and also from (A9) at time $t/2$, and the agreement of

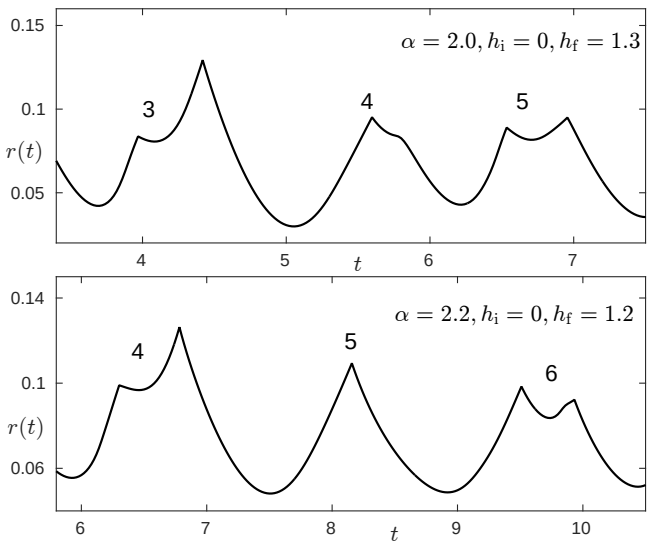

Figure 10. Examples of double cusps for quenches within the anomalous phase. Here for $\alpha = 2$, the 3rd and 5th cusp are double cusps, for $\alpha = 2.2$ the 4th and 6th cusps are double cusps.

both serves as an additional check for the validity of the numerical results.

Appendix B: Additional Rate Function Plots

1. Double Cusps

In this section we show examples of anomalous double cusps, that show up for quenches with $\alpha \lesssim 2.3$ and $h_\mathrm{f} < h_\mathrm{c,z}^\mathrm{II}$. Some of the anomalous cusps develop a double cusp structure in the sense that the tip of these cusps seems to be cut off by another rate-function branch coming down at exactly that time.

2. Crossover between Regular and Anomalous Cusps

In this section we describe for quenches with $\alpha \lesssim 2.3$ and $h_\mathrm{i} = 0$, how regular cusps overtake the anomalous cusps with h_f approaching and going over $h_\mathrm{c,z}^\mathrm{II}$. As mentioned in the main text, this is due to a new group of rate-function branches $r_i(t)$ (A7) coming down with increasing h_f, which eventually become lower than the branches responsible for developing the anomalous cusps. This new group of rate-function branches then start to develop regular cusps between each other for all $h_\mathrm{f} > h_\mathrm{c,z}^\mathrm{II}$. Such a crossover situation is depicted in Fig. 11 for $\alpha = 2$. Further increasing h_f will cause all anomalous cusps to be completely covered by these new branches, which develop regular cusps. The anomalous cusps could in principle still be followed and identified in the higher up rate-function branches, but they do not contribute to the actual return rate function $r(t)$ and cusps therein anymore.

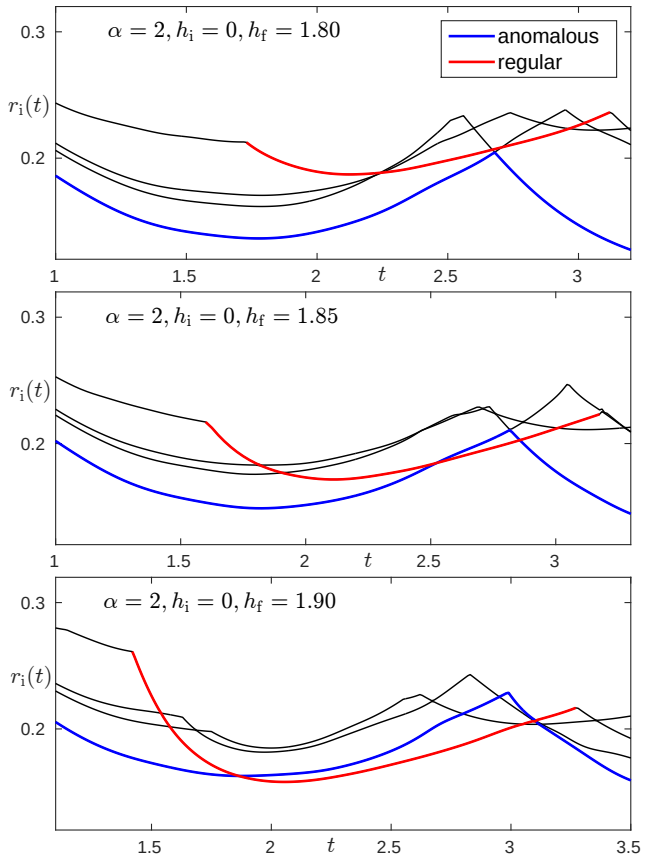

Figure 11. Example of rate-function branches $r_i(t)$ responsible for developing regular cusps (red) coming down and taking over branches responsible for developing anomalous cusps (blue) with increasing h_f (here $h_\mathrm{c,z}^\mathrm{II} = 1.85$).

[1] P. Calabrese, F. H. L. Essler, and M. Fagotti, Phys. Rev. Lett. **106**, 227203 (2011).
[2] J. C. Halimeh, V. Zauner-Stauber, I. P. McCulloch, I. de Vega, U. Schollwöck, and M. Kastner, arXiv:1610.01468 (2016).
[3] M. Heyl, A. Polkovnikov, and S. Kehrein, Phys. Rev. Lett. **110**, 135704 (2013).
[4] M. Heyl, Phys. Rev. Lett. **113**, 205701 (2014).
[5] M. Heyl, Phys. Rev. Lett. **115**, 140602 (2015).
[6] M. Heyl, arXiv:1608.06659.
[7] S. Campbell, arXiv1608:05325v1.
[8] B. Zunkovic, A. Silva, and M. Fabrizio, Phil. Trans. R. Soc. A **374**, 20150160 (2016).

[9] E. Canovi, P. Werner, and M. Eckstein, Phys. Rev. Lett. 113, 265702 (2014).
[10] C. Karrasch and D. Schuricht, Phys. Rev. B **87**, 195104 (2013)
[11] N. Fläschner et al., arXiv:1608.05616.
[12] F. Andraschko and J. Sirker, Phys. Rev. B **89**, 125120 (2014).
[13] S. Vajna and B. Dóra, Phys. Rev. B **89**, 161105(R) (2014).
[14] N. Abeling and S. Kehrein, Phys. Rev. B **93**, 104302 (2016).
[15] A. Dutta and J. K. Bhattacharjee, Phys. Rev. B **64**, 184106 (2001).
[16] M. Fannes, B. Nachtergaele, R. Werner, Comm. Math. Phys. **144**, 443 (1992)
[17] F. Verstraete, V. Murg, J.I. Cirac, Adv. Phys. **57**, 143 (2008)
[18] G. Vidal, Phys. Rev. Lett. **93**, 040502 (2004)
[19] A. J. Daley, C. Kollath, U. Schollwck, G. Vidal, J. Stat. Mech.: Theor. Exp. P04005 (2004)
[20] S.R. White, A.E. Feiguin, Phys. Rev. Lett. **93**, 076401 (2004)
[21] The equilibrium critical line has been obtained by monitoring the order parameter $\langle\sigma^z\rangle$ as a function of h in an iMPS groundstate calculation.[22,23]
[22] S. R. White, Phys. Rev. Lett. **69**, 2863 (1992).
[23] I. P. McCulloch, arXiv:0804.2509, (2008)
[24] B. Zunkovic, M. Heyl, M. Knap, and A. Silva, arxiv:1609.08482 (2016).
[25] U. Schollwöck, Ann. Phys. (NY) **326**, 96 (2011).
[26] J. Haegeman et al., arXiv:1408.5056 (2014)
[27] J. Haegeman et al., Phys. Rev. Lett. **107**, 070601 (2011)
[28] F. Verstraete, J.J. Garcia-Ripoll, J.I. Cirac, Phys. Rev. Lett. **93**, 207204 (2004);
[29] I.P. McCulloch, J. Stat. Mech.: Theor. Exp. (2007) P10014;
[30] B. Pirvu, V. Murg, J.I. Cirac, F. Verstraete, New J. Phys. **12**, 025012 (2010)
[31] G.M. Crosswhite, D. Bacon, Phys. Rev. A **78**, 012356 (2008); G.M. Crosswhite, A.C. Doherty, G. Vidal, Phys. Rev. B **78**, 035116 (2008); F. Fröwis, V. Nebendahl, W. Dür, Phys. Rev. A **81**, 062337 (2010)
[32] L. Michel, I.P. McCulloch, arXiv:1008.4667 (2010)
[33] Higher order schemes can be constructed in a slightly different way, but are computationally much more unfavorable than performing a first order step several times for a smaller time step.
[34] J. Haegeman, V. Zauner-Stauber, M. Fishman, F. Verstraete, *in preparation*
[35] N. Schuch, M.M. Wolf, K.G.H. Vollbrecht, J.I. Cirac, New J. Phys. **10**, 033032 (2008).
[36] T. Prosen, M. Znidaric, Phys. Rev. E **75**, 015202 (2007)
[37] The gauge choices for $A^s(0)$ and $A^s(t)$ do not affect the eigenspectrum of $\mathcal{T}(t)$ and are therefore irrelevant.
[38] V. Zauner et al., New J. Phys. **17**, 053002 (2015)